Japanese Journal of
Applied Physics

The Japan Society of Applied Physics

ACCEPTED MANUSCRIPT

Particle transport in sputter deposition process using argon or krypton gas: effect of thermalization on deposition rate and thickness uniformity

To cite this article before publication: Takeo Nakano *et al* 2026 *Jpn. J. Appl. Phys.* in press https://doi.org/10.35848/1347-4065/ae4309

Particle transport in sputter deposition process using argon or krypton gas: effect of thermalization on deposition rate and thickness uniformity

Takeo Nakano[1]*, Soga Maeda[1], and Md. Suruz Mian[2]

[1] *Faculty of Science and Technology, Seikei University, Musashino, Tokyo 180-8633, Japan*

[2] *School of Engineering, Tokai University, Hiratsuka, Kanagawa 259-1292, Japan*

*E-mail: nakano@st.seikei.ac.jp

The effects of sputtering gas on particle transport in DC magnetron sputtering have been studied. Using argon or krypton as sputtering gas, Al, Ti, Cu, or Mo targets were sputtered at gas pressures ranging from 0.5 to 20 Pa. The deposition rates at the front face were almost constant at low gas pressures, then decreased above a certain pressure. The thickness uniformity deteriorated with increasing gas pressure, and the backside deposition reached its maximum at the boundary pressure. The dependence of these behaviors on the gas and target materials was examined using thermalization behavior evaluated by Monte Carlo simulation.

The gas pressure during magnetron sputter deposition is known to affect the properties of the deposited film significantly.[1,2]. It is due to the behavior of sputtered particles: they initially have high kinetic energy of several eV, but are decelerated by collisions and scattering with the sputtering gas, reaching a low energy corresponding to the gas temperature ("thermalization"). The particle energy induces various phenomena during the deposition,[3] such as enhancement of adatom migration and dislocation formation through recoil implantation. The film structure[4] and properties[5] are modified by these effects.

Thermalization also affects the deposition rate and the thickness uniformity on the substrate because the transport behavior of sputtered atoms exhibits two distinct modes.[6] Before thermalization, the transport mode is called "ballistic", in which the gas motion is negligible because the sputtered particles are much faster. On the other hand, after thermalization, the mode is called "diffusive", where the sputtered particles are driven by the density gradient. In this case, a perfectly absorbing chamber wall imposes a zero density boundary condition,[7] strongly affecting the particle transport and delivery.

Because of the importance of the thermalization of sputtered particles, it has attracted the interest of many researchers since the late 1970's[8] and has been studied mainly through computer simulations by many researchers[9–15]. We have also developed a method that rigorously treats the thermal motion of colliding gases under the Maxwell distribution.[16] It enabled tracking the deceleration process of sputtered particles until thermalization.

The distance from the target at which the majority of sputtered particles are thermalized is called the "thermalization distance." Since the thermalization is governed by the number of collisions with gas particles, the thermalization distance d is considered proportional to the mean free path and inversely proportional to the gas pressure p. Therefore, the pd product value is a specific value for the element of sputtered atoms, their initial energy distribution, the gas element, and gas temperature. We have proposed a method[17] to evaluate the pd value using our Monte Carlo simulation framework. The pd values for several metals with different atomic masses (Al, Cu, Mo) in Ar are calculated to be 7~15 Pa cm, and the lighter the target atom is, the shorter the pd value is. These findings were consistent with our experimental studies, in which we evaluated the dependencies of the deposition rate and thickness uniformity on gas pressure and the target-to-substrate (T-S) distance.[18,19] The experiment was conducted using argon as a sputtering gas. It was demonstrated that, for lighter-atom-mass targets, a decrease in deposition rate, a change in their T-S distance dependence, and deterioration in thickness uniformity occurred at lower gas pressures.

It is also expected that the transport process can be altered by changing the sputtering gas.

It is because the mass ratio of the sputtered particle to the gas atom governs the scattering and deceleration processes in collisions. Actually, Rossnagel also demonstrated the effect of sputtering gas species on the transport process in his 1990 paper.[6)]

Among inert gases, krypton is the most widely used alternative to argon for sputter deposition. In the sputter-deposition of a silver film, it was shown that Kr use helped lower the resistivity.[20,21)] It was ascribed to the suppression of reflecting high-energy neutrals.[22)] That is, the heavier the mass of the incident gas ion is, the lower its energy becomes when it is neutralized and reflected at the target. Krypton is also preferred for sputter deposition of non-evaporable getter coatings for UHV applications.[23–25)] It is because, in argon sputtering, a non-negligible amount of Ar atoms are incorporated into the deposited layers, probably originating from the high-energy Ar neutrals. This kind of improvement has also been reported for high-power impulse magnetron sputtering of tungsten.[26)] In any case, how sputtered particles are transported in different kinds of gases and how they affect the deposition rate distribution is a crucial issue. While these advantages are often discussed from the viewpoint of energetic neutrals, the gas species also changes the thermalization and transport of sputtered atoms, which directly influence the deposition rate and thickness uniformity.

In this study, we have experimentally elucidated the transport process of sputtered particles in Ar or Kr by measuring the pressure dependence of deposition rate, thickness uniformity, and backside deposition in cases of sputter deposition of Al, Ti, Cu, or Mo. They were chosen to cover a wide range of atomic masses, including elements lighter than Ar and heavier than Kr (their atomic masses are summarized in Table S2 of the supplementary data). Furthermore, sputter deposition of these metals is widely used across various applications. The thermalization pd values for combinations of sputtering gas and sputtered material were estimated using the Monte Carlo method and used to interpret the experimental results.

The sputtering experiment was conducted with the same apparatus previously reported.[18)] The sputter chamber is a cylinder with a 210 mm diameter and 250 mm in height. A two-inch sputter gun is located along its axis of symmetry. The chamber was routinely evacuated to 2×10^{-5} Pa after bakeout using a turbomolecular pump prior to each experiment. Argon or krypton gas was fed into the chamber at 10 sccm via a mass-flow controller, and the evacuation valve was throttled to achieve a gas pressure of 0.5-20 Pa. The pressure was measured by a capacitance manometer (MKS Baratron 626A).

The deposition rate was measured using quartz crystal microbalances (QCMs) at three positions: two at the front face of the holder, corresponding to the center and edge of the

substrate, and one at the back face. The schematic of the target and the QCM holder is illustrated in Fig. 1. The "center" QCM (C) and the "edge" QCM (E) are separated by 28 mm. In this study, the "thickness uniformity" was evaluated using the ratio E/C of the deposition rates of two front-face QCMs. A ratio close to unity indicates good thickness uniformity, whereas a deviation reflects non-uniform deposition. The "back" QCM (B) is also located 28 mm away from the symmetric axis. The distance between the target and the QCM holder, which corresponds to the target to substrate (T-S) distance, is variable and was set to 40 or 60 mm in this study. The QCMs were monitored using a multi-channel monitor (Inficon, SQM-160). It records thickness at 0.1 nm resolution. The deposition rate in this experiment was obtained from the slope of the thickness vs time data.

The Al, Ti, Cu, or Mo target with a purity of 3N (Ti) or 4N (other) with a 50 mm diameter and a 3 mm thickness (supplied by Furuuchi Kagaku) was placed on the sputter gun, and a discharge power of 50 W was applied by a DC power source (Heiwa denki, DCS700-0.8). The fresh target was sputtered for more than 30 min, and after confirming discharge-voltage stabilization, the deposition measurement was conducted. DC voltages of each condition (target metal, sputtering gas, and its pressure) are given in Table S1 in the supplementary data.

Figure 2 shows the deposition rates of eight pairs of the target (Al, Ti, Cu, and Mo) and the gas (Ar or Kr) at different gas pressures at the T-S distance of 40 mm. The complete data set, including the T-S distance for 60 mm cases, is available in the Figs. S1-S8 in supplementary data.

The pressure dependence of the deposition rate can be separated into two regions. At lower pressures, the deposition rate at the front-face QCMs (C and E) is almost constant, whereas the rate at B increases with pressure. On the other hand, at higher gas pressures, the rates at C and E decrease with an increase in pressure. In this region, the decrease at E becomes more abrupt, suggesting a degradation in the uniformity of the substrate thickness. At B, the deposition rate also decreases, resulting in a maximum at the boundary of these two regions.

The origin of these behaviours has been discussed in our previous paper,[18] which used only argon as the sputtering gas. The description of the maximum at B was as follows: at low pressures, sputtered particles in ballistic transport change direction through collisions with gas; thus, increased pressure leads to a greater deposition rate on the hidden back surface. However, as pressure increases further, thermalization begins, and the region shrinks toward the target. In this case, the boundary effects in diffusion transport make it difficult for particles to reach the back surface. Namely, the zero-density boundary condition

effectively confines the diffusing flux near the target-facing region, reducing the probability of reaching shadowed locations such as the backside. The deterioration in deposition rate and its uniformity at the front face can also be understood in this context. The return of the sputtered particles toward the sputter gun should also contribute to the decrease in deposition rate at higher pressures.

The boundary pressure of the two regions at which the rate of B is maximum was found to be affected by the target element. The lower the atomic mass of the target element was, the lower the boundary pressure became. It was in agreement with the order of the pd value estimated by the Monte Carlo simulation method.[17)]

In this study, in addition to the target element, the sputtering gas was alternated between Ar and Kr, and the effect of these combinations on the pressure dependence of the deposition rate was investigated. As shown in Fig. 2, when Kr was used as the sputtering gas, the boundary pressure decreased for all metal targets. The larger, heavier krypton atom is expected to have greater "stopping power" than Ar, and it was observed that the reduction in deposition rate began at a lower gas pressure in Kr than in Ar.[27)]

To discuss the dependence of target and gas elements on the boundary pressure more quantitatively, the pd values for thermalization were calculated for the combinations used in the experiment and shown in Fig. 3. They were obtained using the Monte Carlo method we proposed earlier. [17)] A summary of the method, along with the parameters used in the calculation (Table S2) and obtained pd values (Table S3), is provided in the supplementary data. To visualize the effect of the ratio between the atomic mass of the target M_t and that of the sputtering gas ion (projectile) M_p, the pd value was plotted as a function of M_t/M_p. Such mass ratios were considered to significantly influence the scattering angle and the energy decay of sputtered particles in binary collisions with the gas, particularly during ballistic transport. Namely, the lighter atom can be backscattered by the gas, while the heavier atom is not. When the M_t/M_p is close to unity, the kinetic energy transfer occurs efficiently, making the energy decay of sputtered particles after collision more pronounced.

It is clear from Fig. 3 that the pd does not depend solely on the mass ratio. The collision cross section for sputtered particles is expected to be larger for Kr than for Ar. Therefore, momentum-transfer collisions occur more frequently in Kr, thereby reducing the pd value. Accordingly, the ratio of pd values $pd_{\mathrm{M,Ar}}/pd_{\mathrm{M,Kr}}$ for the same target and different gases did not show the same value, and became smaller for lighter elements. We do not have a clear explanation for this, but the atomic size of the sputtered particle may contribute to this difference.

It should also be noted that Ti exhibited a larger pd value than the trend line. It may be attributed to the larger binding energy of Ti metal (4.85 eV) compared to Al (3.39 eV) and Cu (3.49 eV). It results in higher initial energy for sputtered particles, as determined by Thompson's formula[28] used in the simulation.

The boundary pressure, which corresponds to the pressure causing the decrease in C and E, or the maximum in B, in Fig. 2, shows good agreement with the pd values shown in Fig. 3, considering a T-S distance of 40 mm. For Al, the shift in boundary pressure due to the difference in sputtering gas was more subtle than that for Cu or Mo. Anyway, in sputter deposition using Kr with a typical apparatus with a T-S distance of 5 to 10 cm, it should be recognized that thermalization may be dominant at pressures of 1 or 2 Pa, even with a heavy-atomic-mass target such as Mo. At this pressure threshold, the incident energy of sputtered particles onto the substrate also changes significantly, and consequently, the microstructure of the resulting film should be strongly affected.

The deposition rate difference at each target with different gases can be attributed to differences in sputtering yield among those combinations. By comparing the energy dependence of the sputtering yield given in the book,[29] argon produces a higher sputtering yield than Kr at energies corresponding to the discharge voltage observed in this study. The only exception is Al, where Ar and Kr show nearly the same sputtering yields in this energy range. The experimentally observed faster deposition rate of Ar than Kr at low pressures may be due to Kr's greater scattering strength for sputtered particles.

In summary, we investigated the pressure dependence of the deposition rate, thickness uniformity, and backside deposition in DC magnetron sputtering using Ar or Kr for Al, Ti, Cu, and Mo targets. A clear transition in the pressure dependence of the deposition rate, reflecting the transport of sputtered particles, was observed in all combinations. The boundary pressure depended on both the target and the gas species and decreased when Kr was used. The tendency was consistent with the thermalization pd values estimated by Monte Carlo simulations. These results indicate that the thermalization criterion provides a practical framework for interpreting gas-dependent transport and a simple guideline: the transition pressure is roughly estimated by $p \approx (pd)/L$, where L is the target-to-substrate distance. For typical L of several centimeters, thermalization can become significant even at 1-2 Pa with Kr.

Acknowledgments

The krypton gas was provided by Air Liquide Laboratories.

References

1) J. A. Thornton, J. Vac. Sci. Technol. **11**, 666 (1974).
2) J. A. Thornton, J. Vac. Sci. Technol. A **4**, 3059 (1986).
3) D. M. Mattox, J. Vac. Sci. Technol. A **7**, 1105 (1989).
4) A. Anders, Thin Solid Films **518**, 4087 (2010).
5) S. M. Rossnagel and J. J. Cuomo, Thin Solid Films **171**, 143 (1989).
6) S. M. Rossnagel, IEEE Trans. Plasma Sci. **18**, 878 (1990).
7) John. Crank, *The mathematics of diffusion* (Oxford University Press, Oxford, 1986) Second Edition.
8) J. H. Keller and R. G. Simmons, IBM J. Res. Dev. **23**, 24 (1979).
9) R. E. Somekh, J. Vac. Sci. Technol. A **2**, 1285 (1984).
10) T. Motohiro and Y. Taga, Surf. Sci. 134, L494 (1983).
11) G. M. Turner, I. S. Falconer, B. W. James and D. R. McKenzie, J. Appl. Phys. **65**, 3671 (1989).
12) A. Bogaerts, M. van Straaten and R. Gijbels, J. Appl. Phys. **77**, 1868 (1995).
13) D. Depla and W. P. Leroy, Thin Solid Films **520**, 6337 (2012).
14) V. A. Volpyas, A. Y. Komlev, R. A. Platonov and A. B. Kozyrev, Phys. Lett. A **378**, 3182 (2014).
15) A. Revel, A. El Farsy, L. de Poucques, J. Robert and T. Minea, Plasma Sour. Sci. Technol. **30**, 125005 (2021).
16) T. Nakano, I. Mori and S. Baba, Appl. Surf. Sci. **113/114**, 642 (1997).
17) T. Nakano and S. Baba, Jpn. J. Appl. Phys. **53**, 038002 (2014).
18) T. Nakano and S. Baba, Vacuum **80**, 647 (2006).
19) T. Nakano, R. Yamazaki and S. Baba, J. Vac. Soc. Jpn. **57**, 152 (2014).
20) M. Kawamura, R. Sagara, Y. Abe, T. Kiba and K. H. Kim, Jpn. J. Appl. Phys. **59**, 048001 (2020).
21) R. Sagara, M. Kawamura, T. Kiba, Y. Abe and K. H. Kim, Surf. Coat. Technol. **388**, 125616 (2020).
22) Y. Takagi, Y. Sakashita, H. Toyoda and H. Sugai, Vacuum **80**, 581 (2006).
23) C. Benvenuti, P. Chiggiato, P. Costa Pinto, A. Escudeiro Santana, T. Hedley, A. Mongelluzzo, V. Ruzinov and I. Wevers, Vacuum **60**, 57 (2001).
24) C. Zhou, D. Li, Y. He, Z. Ma and L. Yang, AIP Adv. **13**, 055221 (2023).
25) X. Liu, M. Adam, Y. He and Y. Li, in *Proc. 2005 Particle Accelerator Conference* (IEEE, Knoxville, USA, 2005) pp. 2860.

26) T. Shimizu, K. Takahashi, R. Boyd, R. P. Viloan, J. Keraudy, D. Lundin, M. Yang and U. Helmersson, J. Appl. Phys. **129**, 155305 (2021).

27) I. Petrov, I. Ivanov, V. Orlinov and J.-E. Sundgren, J. Vac. Sci. Technol. A **11**, 2733 (1993).

28) M. W. Thompson, Nucl. Instrum. Methods Phys. Res. B **18**, 411 (1986).

29) R. Behrisch and W. Eckstein, Eds., *Sputtering by Particle Bombardment: experiments and computer calculations from threshold to MeV energies* (Springer, Berlin, 2007).

Figures

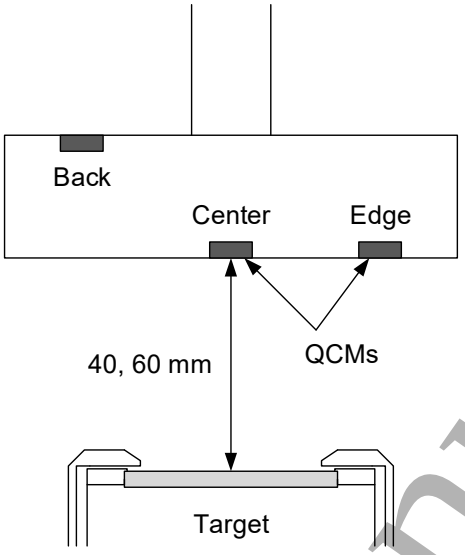

Fig. 1. Schematics of the deposition rate measurement setup. Two QCMs were located on the target-facing side of the holder, and another QCM was on the back side. The aperture of the QCMs was 8 mm. The center of the Edge or Back QCM was 28 mm away from the symmetric axis. The distance between the target and the holder was set to 40 or 60 mm in this study.

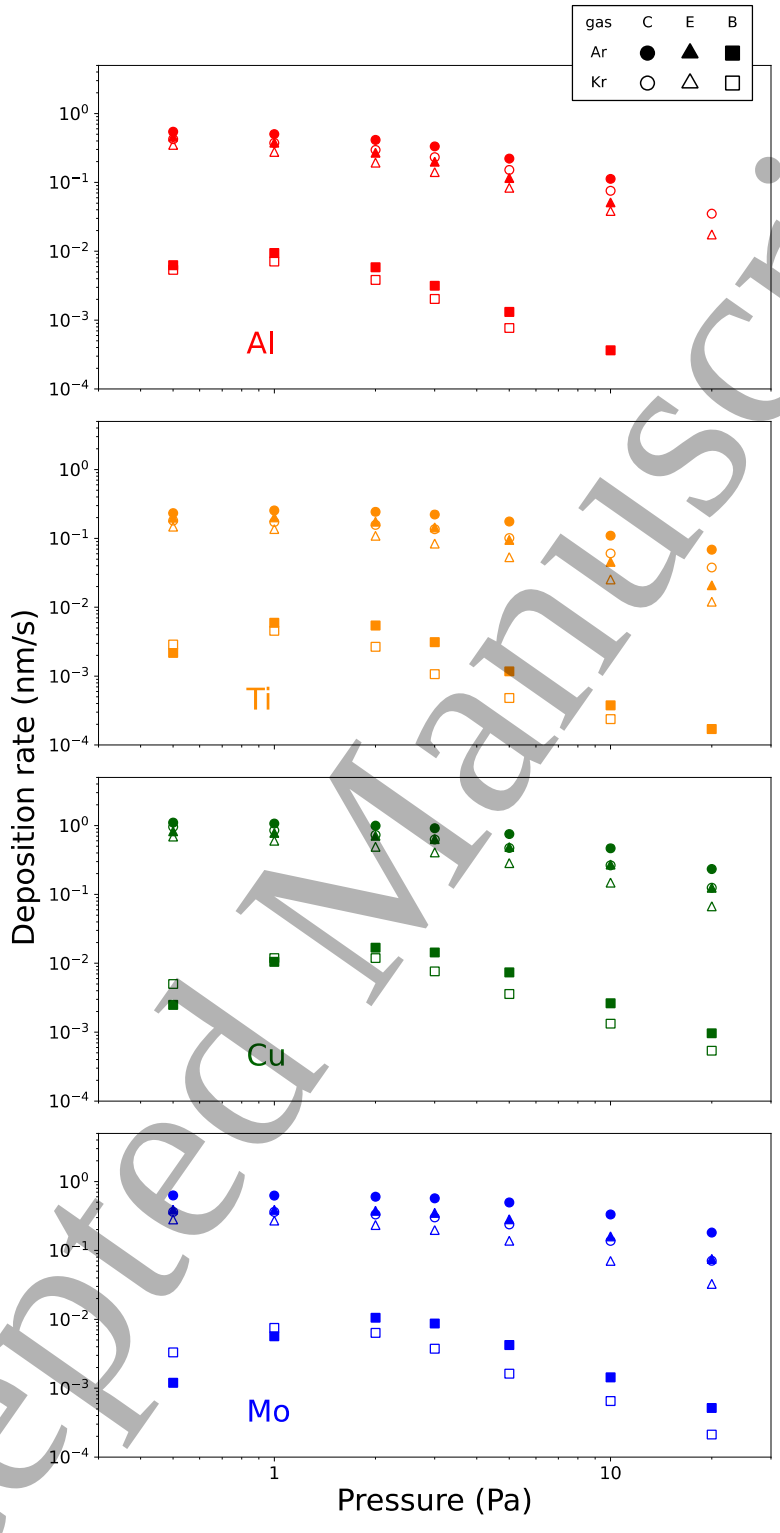

Fig. 2. Deposition rate at the Center, Edge, and Back QCMs measured with different target metals and sputtering gases at the target-to-substrate distance of 40 mm. Note that the vertical axes are given in a logarithmic scale. Filled markers denote results with Ar gas, and open markers denote results with Kr gas.

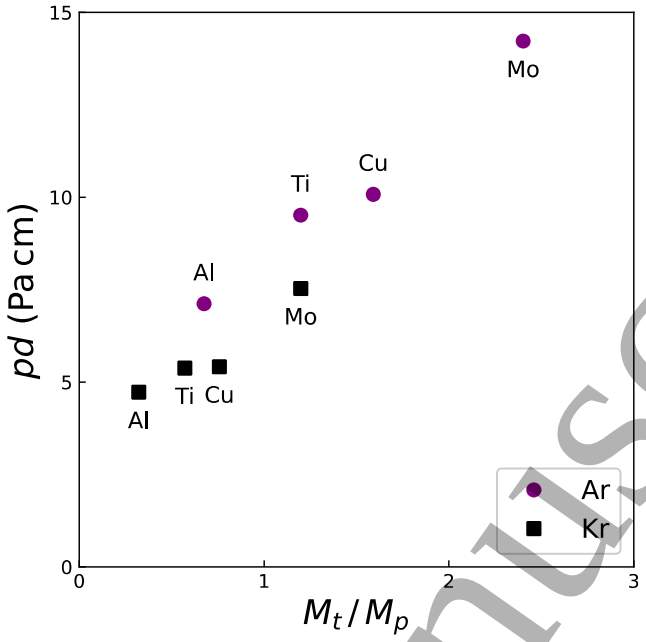

Fig. 3. Calculated pd values obtained by the Monte Carlo method for the pairs of metals and gases used in this study, plotted as a function of M_t/M_p, where M_t and M_p are the atomic mass of the target metal and projectile gas ions, respectively.